Region of Freshwater Influence (ROFI) and its impact on sediment transport in the Lower Mekong Delta Coastal Zone of Vietnam

Nguyet-Minh Nguyen[1], Dinh Cong San[1], Kim Dan Nguyen[2], Quoc Bao Pham[3], Alexandre S. Gagnon[4], Son T. Mai[5], Duong Tran Anh[6*]

[1] Southern Institute of Water Resources Research, Ho Chi Minh City, Vietnam

[2] Laboratory for Hydraulics Saint-Venant, Université Paris-Est, 6 Quai Wattier, 78400 Chatou, France

[3] Institute of Applied Technology, Thu Dau Mot University, Binh Duong province, Viet Nam

[4] School of Biological and Environmental Science, Liverpool John Moores University, Liverpool L3 3AF, United Kingdom

[5] School of Electronics, Electrical Engineering and Computer Science, Queen's University Belfast, United Kingdom.

[6] HUTECH University, 475A Dien Bien Phu Street, Binh Thanh District, Ho Chi Minh City, Vietnam

* Corresponding author: Duong Tran Anh (ta.duong@hutech.edu.vn)

Abstract

The delta of the Mekong River is one of the largest in the world, with the Mekong River carrying large amount of sediments in its Region of Freshwater Influence (ROFI). This study investigates the flow structure and movement of both suspended and bedload sediments in the ROFI of the Lower Mekong Delta (LMD) in order to identify areas prone to sediment accretion and erosion. This is accomplished by applying the three dimensional Coastal and Regional Ocean COmmunity (CROCO) model and then calculating the sediment budget of different stretches of the coastline. The model outputs, depicting areas experiencing sediment accretion and erosion along the coastline of the LMD, are then compared against observations obtained during the period 1990-2015 and demonstrate the ability of the model to identify areas particularly prone to erosion and where preventive actions against coastal erosion should focus.

Key words: Accretion and erosion; CROCO model; ROFI; sediment transport; Mekong Delta

1. Introduction

The Mekong Delta in southern Vietnam hosts a population of over 17 million people (Buschmann *et al.*, 2008). It is an important region for agriculture and aquaculture, producing over 55% of the rice crop of the country and over 60% of its seafood (Guong and Hoa, 2012), in addition to being a hotspot of biodiversity, the second in the world after the Amazon basin (Ziv *et al.*, 2012; Campbell, 2012). The Mekong Delta region, however, is facing many challenges such as an expansion of hydropower development across the Mekong River Basin, which has led to a significant reduction to the supply of sediments entering the delta (Cochrane *et al.*, 2014; Kondolf *et al.*, 2014), causing coastal erosion (Li *et al.*, 2017; Le Xuan *et al.*, 2019),

The Mekong is among the largest rivers worldwide; the eighth largest river in terms of its discharge and the tenth most important for its sediment load (Meade, 1996; Li *et al.*, 2017). The average annual discharge of the Mekong River is approximately 12,500 m^3/s, although it experiences strong seasonal variations, with a ratio of maximum to minimum discharge in a year of around six to eight. This volume of freshwater contributes to an important and seasonally variable buoyancy plume to an extensive region of its coastal zone and adjacent shelf sea, a region referred to as the Region of Freshwater Influence (ROFI) (Simpson, 1997). The ROFI can extend offshore from one kilometre from the Mekong River estuary to several hundred kilometres depending on the magnitude of the river discharge (Geyer & Kineke, 1995; Horner-Devine *et al.*, 2015).

The ROFI of many coastal regions worldwide has previously been investigated, but with a limited number of studies focusing on the Mekong Delta (Fong & Geyer, 2002; De Boer *et al.*, 2006). Both estuarine and shelf sea processes take place in a ROFI (Simpson, 1997; Horner-Devine *et al.*, 2015), with the amount of mixing in the ROFI depending on wind speed and

direction, tidal range, the shape of the estuary and the amount of river discharge. The ROFI of the Mekong Delta thus strongly varies seasonally, depending mainly on the monsoonal winds and the magnitude of the Mekong River discharge (Hordoir *et al.*, 2006), as the Coriolis force is weak at the latitude of the delta (Simpson and Snidvongs, 1998).

Horner-Devine et al. (2009) proposed the following conceptual model of the ROFI. At very low wind speeds, freshwater flows out of the river mouth to form a two-part structure: a baroclinic recirculation bulge near the river mouth and a coastal current. In this situation, the freshwater bulge experiences an anticyclonic circulation and grows indefinitely until altered by an external force such as an ambient current or wind (Figure 1a). When the winds are strong enough, the freshwater plume is influenced by Ekman transport (Price *et al.*, 1987; Wang *et al.*, 2013). Upwelling and downwelling can occur during a tidal cycle as well as on a seasonal scale due to changing monsoon winds (Chen *et al.*, 2012; Hein *et al.*, 2013). Downwelling winds blowing towards the coastline impact the plume dynamics by compressing it against the coast (Figure 1b), while upwelling winds blowing across the ocean surface cause expansion of the freshwater plume sea-ward and detachment of the low salinity water from the plume, erasing the buoyancy signature (Figure 1c). This is because the movement of the freshwater plume offshore due to Ekman transport causes the intrusion of saltier ambient waters on the continental shelf, promoting plume detachment and leaving mixed waters near the coast (Pimenta *et al.*, 2011; Joseph, 2017).

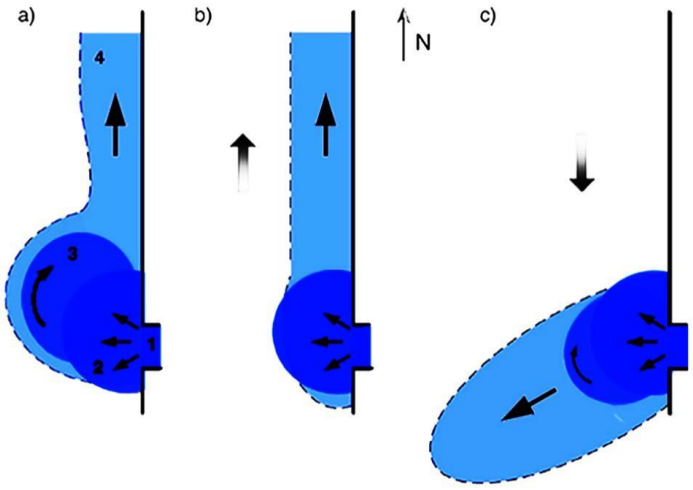

Figure 1. Conceptual model of a ROFI under three different wind forcing conditions: a) freshwater plume during low wind speeds, with numbers 1, 2, 3, and 4 showing the river (source), tidal, bulge, and the far-field parts, respectively, of the river plume; b) freshwater plume under downwelling conditions, which compress the re-circulating and far-field plumes against the coast; and c) freshwater plume under upwelling conditions (adapted from Horner-Devine *et al.* 2009).

Previous studies have investigated the dynamics of river plumes and the ROFI using either laboratory experiments (Thomas & Linden, 2010; Yuan *et al.*, 2018), field measurements (Geyer *et al.*, 2004; Simpson *et al.*, 2005) or numerical models (Whitney & Garvine, 2005; Xing & Chen, 2017). These studies, nonetheless, have to date mainly focused on the structure and dynamics of the freshwater bulge and coastal currents with limited attention paid to salinity variations and sediment transport due to seasonal changes in monsoonal wind (Yao *et al.*, 2016). In that regard, the deposition of fine sediments on the continental shelf during the Southwest (SW) monsoon due to high river discharge has been demonstrated (Thanh et al., 2017; Le Xuan et al., 2019). However, previous studies have also suggested that sediment deposition occurs during the low flow season, but it is limited to areas near the river mouth, where the delta is still expanding, and that the wind driven circulation, waves, and tidal action cause net erosion in other parts of the Lower Mekong Delta Coastal Zone (LMDCZ) during

that season. Even though the net transport of fine sediments at the annual time-scale is to the south, i.e., towards the Gulf of Thailand, there is a negative sediment budget on the coast of that region due to the strong coastal current causing coastal erosion and hence shoreline retreat, evidence for which is presented in Karlsrud et al. (2017). This strong coastal current, flowing in the direction of the propagating Kelvin wave, was also observed in the modelling study of Hordoir et al. (2006) mentioned earlier.

In brief, Hordoir et al. (2006) identified the main processes of the freshwater plume under seasonally varying monsoonal winds, river flow regimes and salinity profiles, but without considering sediment transport, while Hein et al. (2013) investigated the influence of seasonal variations in river discharge and monsoonal winds on the dynamics of suspended sediments, but not that of bedload sediments. Marchesiello *et al.* (2019), for their part, previously applied the CROCO model to the Mekong Delta to investigate sediment dynamics and the associated shoreline change, but they did not consider the influence of seasonal variability in salinity, flow structure and their impact on sediment transport in the ROFI. Besides, they mentioned the importance of considering the re-suspension of sediments caused by the action of waves on the seabed, particularly during the north-easterly winds in the winter, and their subsequent distribution by ocean currents. Studies in other regions have also shown that the ROFI influences not only the transport of suspended sediments but also that of bedload sediments. Therefore, an investigation of the processes and dynamics of the ROFI incorporating sediment transport is recommended in view of recent anthropogenic changes in the basin.

This study aims to improve our knowledge of the structure of the ROFI in the Mekong Delta and its impact on the regional coastal ocean circulation and sediment transport using a three-dimensional model that takes into consideration different forcings, namely the outflow of freshwater from rivers into the estuary, the tides, waves, winds, and the Coriolis force, even

119 though the latter is considered to be minor at the latitude of the study region. By simulating the
120 movement of both suspended and bedload sediments, this modelling study also aims to identify
121 areas prone to sediment accretion and erosion by establishing an updated sediment budget
122 along stretches of the coastline, in view of recent anthropogenic changes in the basin, and to
123 compare that sediment budget with long-term observations.

124

125 ## 2. Methodology

126 ### 2.1. Hydrological, sediment and salinity data

127 Figure 2 depicts the annual cycle of the discharge of the Mekong River at Kratie in Cambodia
128 over a 45-year period extending from 1999 to 2017. The Mekong Delta is located in a tropical
129 climate region dominated by two seasons defined primarily on the basis of precipitation: a wet
130 season typically lasting from June to October, a cool and dry season, and two transition periods
131 from mid-March to mid-May and in October. Accordingly, the highest discharge is typically
132 reached during the South-west monsoon in August-September, which encourages coastal
133 upwelling. This is in contrast to the cool and dry months of November to February when North-
134 easterly winds dominate the region, promoting downwelling events.

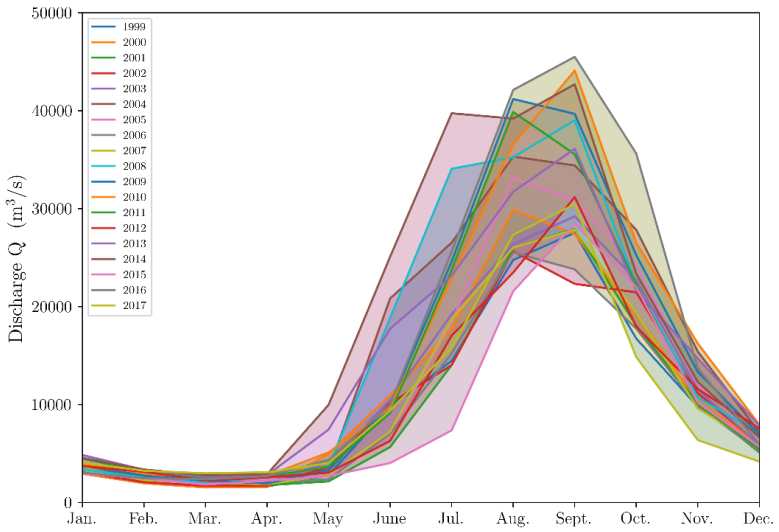

135

136 **Figure 2.** Annual cycle of the Mekong river discharge at Kratie (Cambodia) for all years
137 during the period 1999-2017

Data from two field surveys of 15 days each, one in October 2016 and the other in February-March 2017, conducted as part of the LMDCZ project (SIWWR, 2018), were obtained to validate the model, as described below. During each field survey, two hydrological stations were set up: Go Cong and U Minh (see Figure 1A in the Appendix), and these were supplemented by 183 measurement points taken using two ships, which sailed from Tien Giang on the northern shore of the Mekong River and Kien-Giang in the Gulf of Thailand to Ca-Mau Cape. Data to calculate the significant wave heights and current velocity were collected every 15 minutes at Go Cong and U Minh using FlowQuest Acoustic Current Profilers, while Suspended Particles Matters (SPM) and salinity was measured at the ship measurement points, with one measurement taken at the following depth: 0.2H, 0.4H, 0.6H, 0.8H, where H is the total water depth (m), and on the sea floor using water sample bottles. Each set of measurement lasted 30 minutes.

2.2. Coastal and Regional Ocean Community Model

This study uses version 1.1 of the CROCO model (https://www.croco-ocean.org/), a French model building on the Regional Oceanic Modelling System (ROMS) (Dong *et al.*, 2021). The model solves the primitive equations based on the Boussinesq approximation and the hydrostatic hypothesis (Shchepetkin & McWilliams, 2005; Debreu *et al.*, 2012). It is discretised in geometry, following the curvilinear mesh, with short time steps used to advance the surface elevation and 2D momentum, and larger time steps for solving the 3D momentum equations and the transport equations of scalar variables, i.e., temperature, salinity, and sediment concentration. A third order predictor-corrector algorithm is developed in the code, allowing for a substantial increase in the time step for an efficient integration of realistic configurations of the computational domain, even using fine meshes. A non-local, K-Profile Planetary (KPP) boundary layer scheme (Large *et al.*, 1994) parameterises the unresolved physical vertical sub grid-scale processes, with specific treatment for surface and bottom

boundary layers in shallow water. An active, implicit, upstream-biased radiation condition is used at open-ocean boundaries (Marchesiello *et al.*, 2001). CROCO also includes an accurate pressure gradient algorithm (Shchepetkin & McWilliams, 2003). The hydrodynamic model is therefore developed to simulate both coastal and oceanic regions and their interactions with a high degree of accuracy (Debreu *et al.*, 2016; Soufflet *et al.*, 2016), and is coupled with sediment dynamics from Blaas *et al.* (2007) and Warner *et al.* (2008) to compute sediment transport, erosion, and deposition.

3. Model setup

3.1 Model geometry

The model bathymetry was generated by merging datasets covering the main distributaries, estuaries, and coastal areas using *in situ* measurements and bathymetric data from the General Bathymetric Chart of the Oceans (GEBCO, 2014) at a horizontal resolution of 30 arc-seconds (Figure 3). This domain covers over 744 km of the LMD coastline from Xoai Rap Bay in the Northeast to Ha Tien in the Northwest. The sea open boundaries are located approximately 150-200 km from the coastline at Go Cong and U Minh. The horizontal grid resolution is approximately 500 m, which is less than the Rossby radius in the coastal zone (Hordoir *et al.*, 2006), with 30 sigma layers in the vertical. An initial attempt was also made to use a 10-layer vertical grid to minimise computational time, as described in SIWRR (2018), but the results were not as conclusive and, for this reason, this present paper increase to a 30-layer vertical grid.

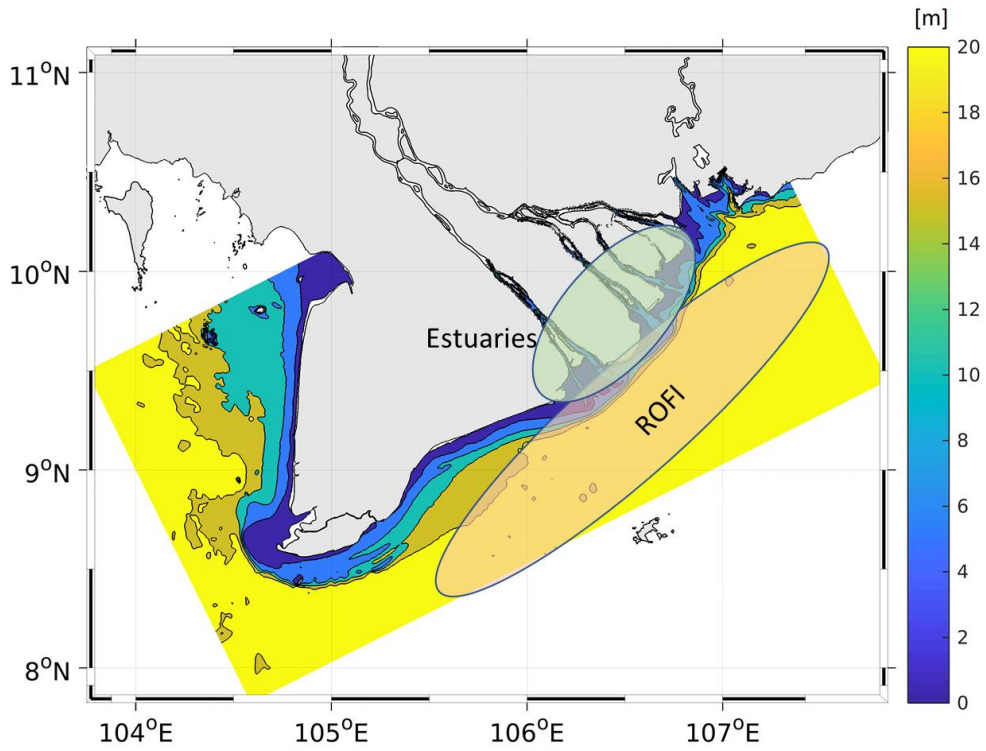

Figure 3. Bathymetry of the study domain with a schematic representation of the ROFI of the Mekong delta and adjacent shelf sea

3.2 Parameterization

Sediment transport was modelled using the multi-class community model embedded within ROMS, which accounts for the influence of waves on sediment transport as well as the interactions between waves and tidal currents. Wave heights were considered in the model by using empirical formulae for wave dissipation and the wave outputs from the ERA-Interim reanalysis. The model followed a multi-class sediment approach and based on laboratory analyses of suspended and bedload sediments collected during field surveys, two classes needed to be considered: silt with a median diameter of 20 μm and a settling velocity of 0.03 mm/s, and sand with a median diameter of 200 μm and a settling velocity of 20 mm/s. The model has a horizontal resolution of 500 m (374x727 pts) and a 30-layers in the vertical (terrain following). Table 1 presents the model configuration variables and their sources including river, tidal, wave and air-sea forcing and sediment parameters.

Table 1. Model configuration variables and their sources

	Parameters	Data source
Topography		Southern Institute of Water Resources Research (SIWRR) data (estuaries, nearshore area) + GEBCO_2014 at 30" (1km)
River forcing	Q, SSC	Discharge and SSC at Can Tho and My Thuan from SIWRR station data
Tidal forcing	u, v, SSH	OSU TPXO8 global solution at 1/30° (~3 km)
Subtidal forcing	u, v, SSH, T, S, SSC	ECCO V2 reanalysis ¼° 3-daily
Air-sea forcing	wind, heat, and freshwater fluxes	ECMWF ERA-Interim at ¼° 6-hourly
Wave forcing	Hs, Dir, T_p	ECMWF ERA-Interim at ¼° 6-hourly; for very shallow areas, the wave height data were modulated using an empirical model of wave dissipation proposed by Grosskopf (1980)
Sediment parameters	D_{50}, Ws	Sand: d50=200 μm; W_s=20-50 mm/s Mud (Floccules): d50=20 μm; W_s=0.03 mm/s

SSH denotes the sea surface height; U and V are the zonal and meridional velocities, respectively; Hs; wave height; Tp: wave period; Dir: wave direction; SSC: suspended sediment concentration, T: temperature, S: salinity, D_{50}: particle diameter at 50% in the cumulative distribution, Ws: Sediment velocity.

3.3 Boundary conditions

The computational domain used for the application of the Coastal and Regional Ocean COmmunity (CROCO) model used upstream discharges at My Thuan on the Tien River and Can Tho on the Hau River, as upstream boundaries, both located about 100 km from the sea.

The tidal boundary conditions were obtained from the TPXO-atlas, while the Estimating the Circulation and Climate of the Ocean (ECCO) reanalysis provided the ocean circulation conditions, including baroclinic forcing (i.e., temperature and salinity). The ECMWF ERA-Interim global reanalysis was used to provide atmospheric forcing to run the model, i.e.., the

total net heat flux and wind stress. The suspended sediment concentration, as measured at Can Tho and My Thuan during 2016-2017, were used as upstream boundary conditions.

4. Model validation

To develop a conceptual structure of the ROFI in the Mekong Delta, the model, after the validation described below, was used to simulate the estuarine and coastal circulations, saltwater intrusion during high tides and sediment transport for the year 2014 using data on the bathymetry, the atmospheric conditions, and the state of the sea (i.e., waves, wind, tidal current). Nonetheless, a longer simulation over a period of two to three years would be preferable to consider the fate of sediments beyond one year, i.e., their deposition, re-suspension, and movement, and research is currently underway to account for this.

Model validation for the significant wave heights at Go Cong during the two field campaigns illustrates a similar comparison for the current velocity at the surface and at the bottom of the sea (see Figure 2A) with Table 2 presenting the level of agreement between the model outputs and the observations using different statistical measures. The correlation between the model simulation and the observations is highest for significant wave height than for velocity, and the correlation (error) was higher (lower) for velocity at U Minh than at Go Cong (Figure 3A).

The CROCO model was also validated using salinity and SPM concentrations measurements taken using a Conductivity, Temperature and Depth (CTD) package of electronic measurements and an Acoustic Doppler Current Profiler (ADCP), respectively, during the two field campaigns mentioned above and field data collected as part of the *VIetnam TELédétection remote sensing* (VITEL) project (IRD, 2014) in June 2014 (see Figure 4).

Table 2. Model performance at the two stations

Parameters and stations	RMSE	MAE	R^2

Significant wave heights in Oct. 2016 at Go-Cong	0.17 m	0.14 m	0.61
Significant wave heights in Feb.-Mar. 2017 at Go-Cong	0.17vm	0.14 m	0.49
Surface velocity in Feb.-Mar. 2017 at U-Minh	0.07vm/s	0.05 m/s	0.35
Bottom velocity in Feb.-Mar. 2017 at U-Minh	0.05 m/s	0.05 m/s	0.35
Surface velocity in Feb.-Mar. 2017 at Go-Cong	0.18 m/s	0.14 m/s	0.21
Bottom velocity in Feb.-Mar. 2017 at Go-Cong	0.16 m/s	0.13 m/s	0.22

RMSE: Root Mean Square Error; MAE: Mean Absolute Error, R^2: coefficient of determinant

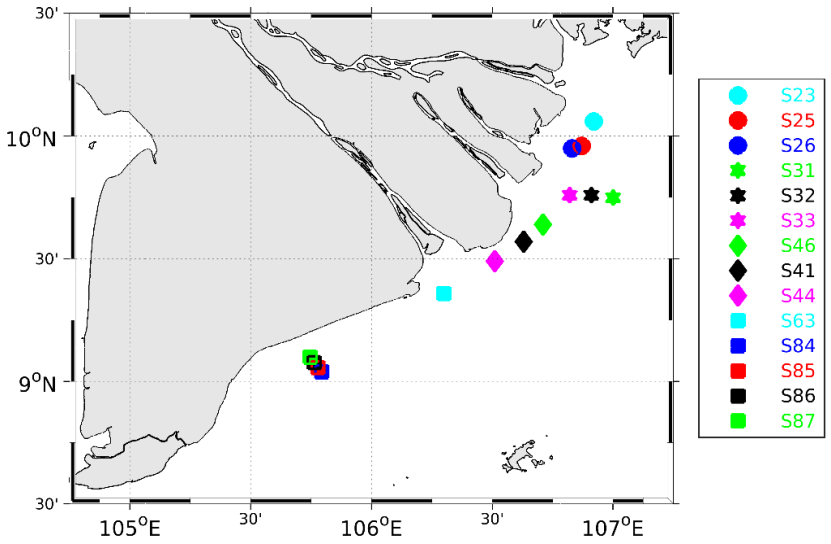

Figure 4. Locations of the salinity profiles and SPM measured by CTD during the VITEL (IRD, 2014) and LMDCZ projects (SIWWR, 2018)

The good agreement of vertical salinity distribution and SPM concentration between measured and simulated results are shown in Figure 4, 5, 6A in the Appendix. Figure 4A and 5A show that the modelled simulation of the salinity profiles compares well with the CTD measurements taken at the different locations. Moreover, these salinity profiles clearly reveal the presence of the ROFI as thin layers of low salinity are observed in the upper part of the vertical profile (less than 5 m from the surface) at some locations, particularly in June when the discharge from the

Mekong River is high due to the rainy season driven by the SW monsoon. Figure 5A, for its part, shows that during the dry season (February-March), the haloclines are weaker and almost non-existent at some locations.

The instantaneous profiles of the computed SPM with the measured ones at a number of stations were shown in Figure 6A. Because the SPM samplings for a vertical profile last 30 minutes, the values measured at different depths of a profile could be not simultaneous. For this reason, a qualitative comparison was preferred for this variable rather than a quantitative one. In general, it is observed that the difference between the simulated and observed SPM is larger at greater depths, refer to S26 and S41 in particular. The simulated SPM is overestimated in comparison to the observed SPM at S31 while it is underestimated at S26 and S41.

Figure 5 shows the freshwater plume, as simulated by the model, during two different wind regimes in 2014: winds encouraging downwelling in January and winds promoting upwelling in July. The shape of the plumes agrees very well with the conceptual model presented in Figure 1, i.e., during the dry period extending from November to February, the freshwater outflow from the Hau River forms a bulge near the river mouth of limited outward extent and a narrow current alongside the coast, as the downwelling conditions compress the current against the coast. In July during the rainy season, however, the strong river discharge and the upwelling wind conditions promote offshore development of the plume.

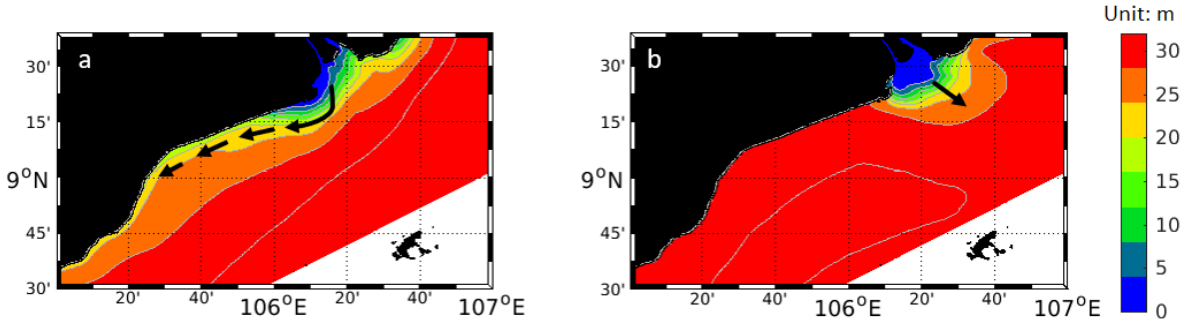

Figure 5. Monthly average freshwater plume at the mouth of the Hau River during the January downwelling winds (left) and the July upwelling winds (right) in 2014.

5. Results and discussion

5.1. Seasonal variability in salinity in the ROFI of the LMDCZ

Figure 6 depicts seasonal variations in the spatial extent of the buoyancy plume during 2014 at Cross-Section CS_3 opposite the mouth of the Hau River at Dinh An and Tran De for the location). From June to the first two weeks of October, the river plume extends 70-90 km offshore because of the large river discharge during the rainy season. This plume creates strong stratification with an approximately 5 m thick freshwater layer, and also contributes to the buoyancy input of the adjacent shelf sea, generating a strong horizontal gradient in salinity. This induces a density-driven circulation with the freshwater at the surface moving offshore and the denser saltwater at the bottom moving shoreward.

Hordoir *et al.* (2006) previously modelled the freshwater plume of the Mekong River to examine its characteristics. The river plume of the Mekong River exhibits strong variability, because of high seasonal variability in river flow and the monsoonal winds (Hein *et al.*, 2013). The major physical processes in the ROFI can be described by the basic competition between buoyancy and stirring, with the latter occurring mainly as a result of wind and tidal motions. From the last two weeks of October to mid-March, north-easterly winds favouring downwelling take place. Freshwater at the surface is directed back towards the coast and forced to sink. The plume extends southward upon leaving the estuaries because of the Coriolis force, and then forms a narrow but strong southward current propagating along the coast as a boundary-trapped Kelvin wave.

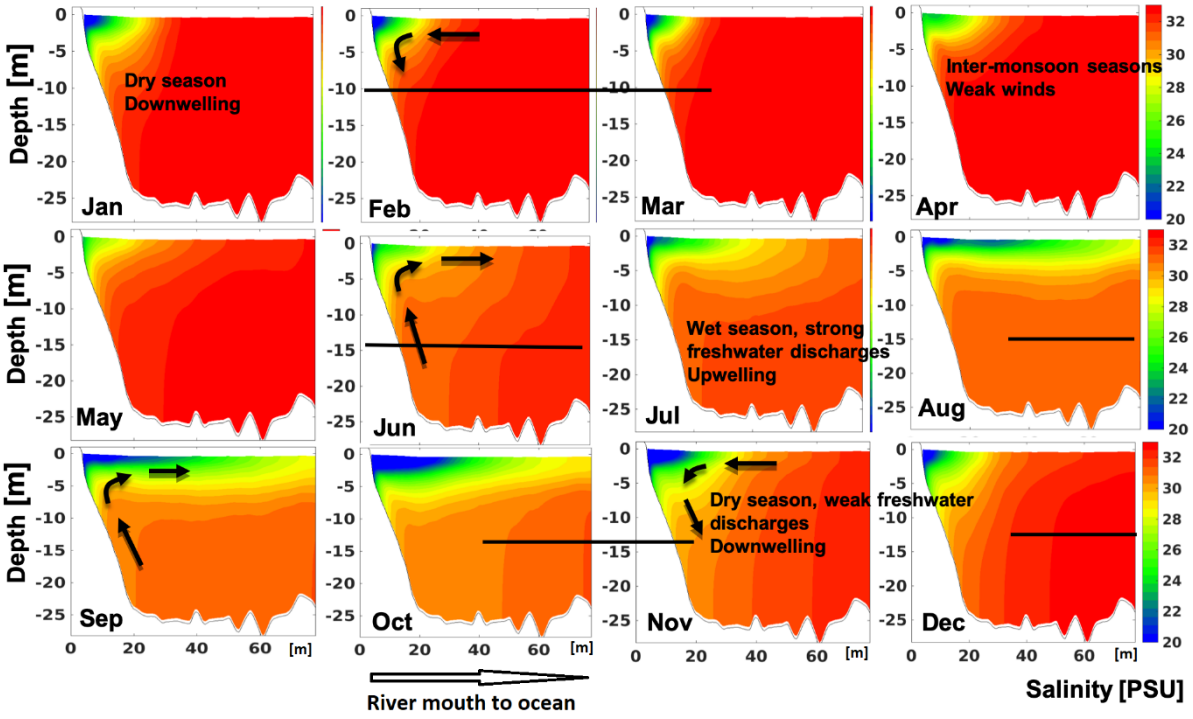

294

295 **Figure 6**. Monthly average salinity profile at cross-section CS_3 for the year 2014.

296 **5.2. Flow structure in the ROFI of the Mekong delta**

297 Figure 7 depicts the monthly average longshore current velocities at CS_3. During the wet
298 season, due to the south-western winds that are favourable to upwelling, large volumes of
299 freshwater flow out of the mouth of the rivers of the Mekong Delta, creating a stratified plume
300 extending offshore in a south-easterly direction. Figure 7 and 8 further show that in proximity
301 to the coast, the longshore currents are in the direction opposite to those of the surface. These
302 south-westerly bottom currents occupy an area extending vertically from the seabed to 5 m
303 from the surface, and horizontally from the coast up to 30 km offshore (Figure 6).

304

305 During the dry season, from mid-October to March, due to the winds from the Northeast
306 promoting downwelling, the freshwater plume is squeezed in a narrow coastal jet about 25-40
307 km wide and 5-7 m thick flowing in a south-westerly direction. This surface coastal jet is most
308 developed in November, when the North-easterly winds are most intense, reaching a velocity
309 of 0.50 m/s and allowing the transport of suspended sediments along the East Coast of Vietnam

in a southerly direction up to Ca Mau Cape, and subsequently carrying them into the West Sea.

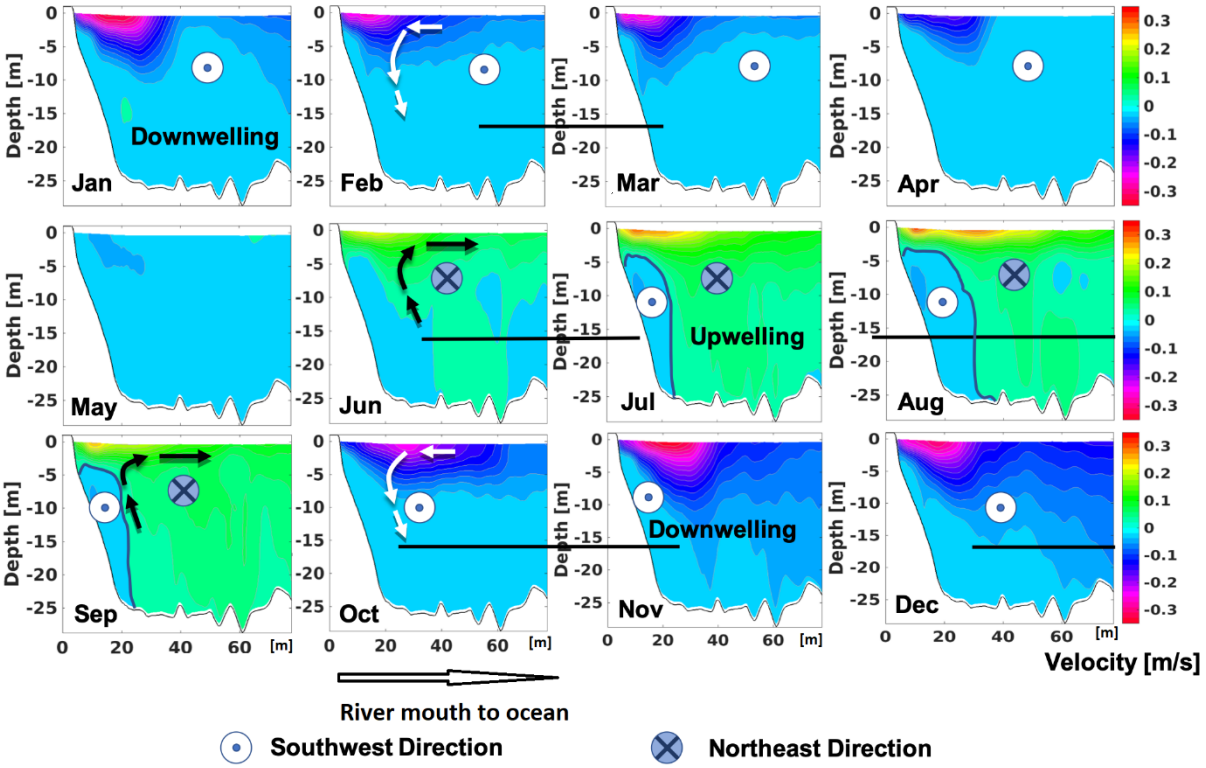

Figure 7. Mean monthly longshore current velocity at CS_3. Negative and positive values refer to South-westerly and North-easterly winds, respectively.

Figures 8 and 9 present the monthly average velocity fields on the surface and at the bottom, respectively, for the year 2014. It reaches maximum level both in intensity (highest velocity) and in extension (largest occupied area) in August and then reduces in intensity and size in September. At the same time, in proximity to the mouth of the Mekong Delta, the bottom currents are opposite to the surface ones, i.e., seawaters flow back to the estuaries. From the last two weeks of October, north-easterly winds, favourable to downwelling, transport surface waters back to the shore. As above, this jet is strongest and extends until the Ca Mau Cape in November. Its intensity reduces in December and reaches its lowest value in April. The bottom currents during the north-easterly winds are in the same direction as the surface ones, but of weaker intensity. Figure 10 provides a schematic representation summarising the flow structure in the LMDCZ on the basic of the model simulations. The

surface and bottom currents are strongly influenced by the wind direction, which resulted in the current directions are depended on wind direction in both seasons. However, the current directions are complex in a zone (top right corner in Figure 9), which can be attributed to a complex topography and influences of river discharge. The seasonal variability of river discharge and monsoon winds has a large influence on water stratification and destratification. Furthermore, the seasonal occurrence of stratification has an effect on the sediment dynamics and ecosystem processes.

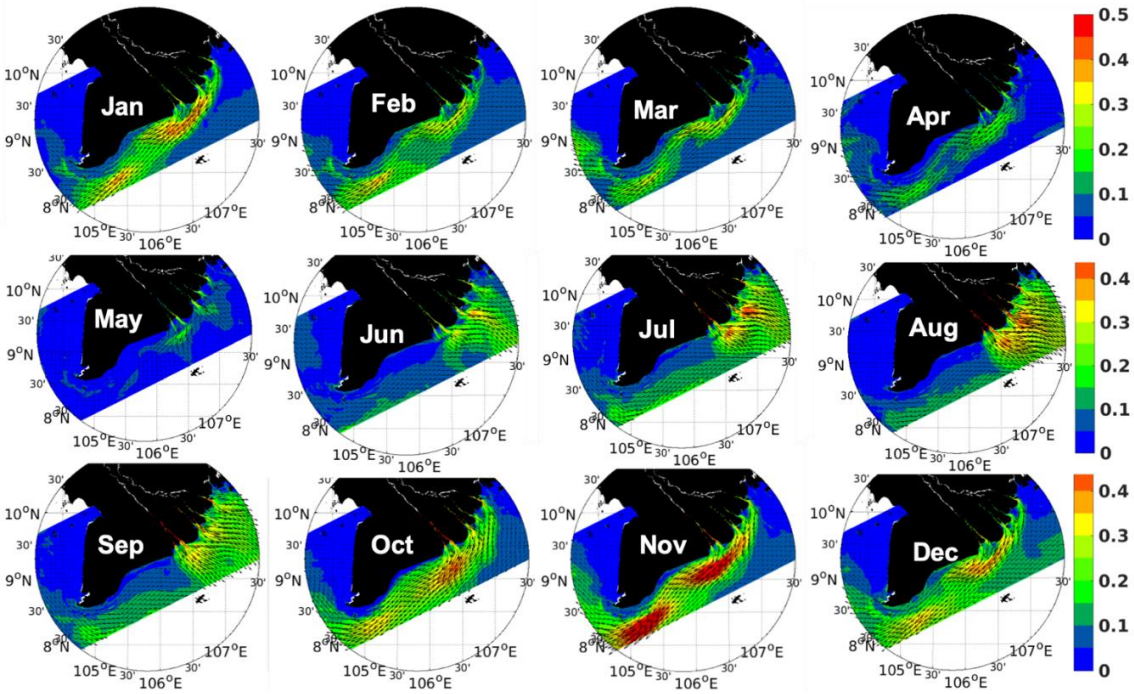

Figure 8. Monthly average surface velocity fields (m/s) in 2014.

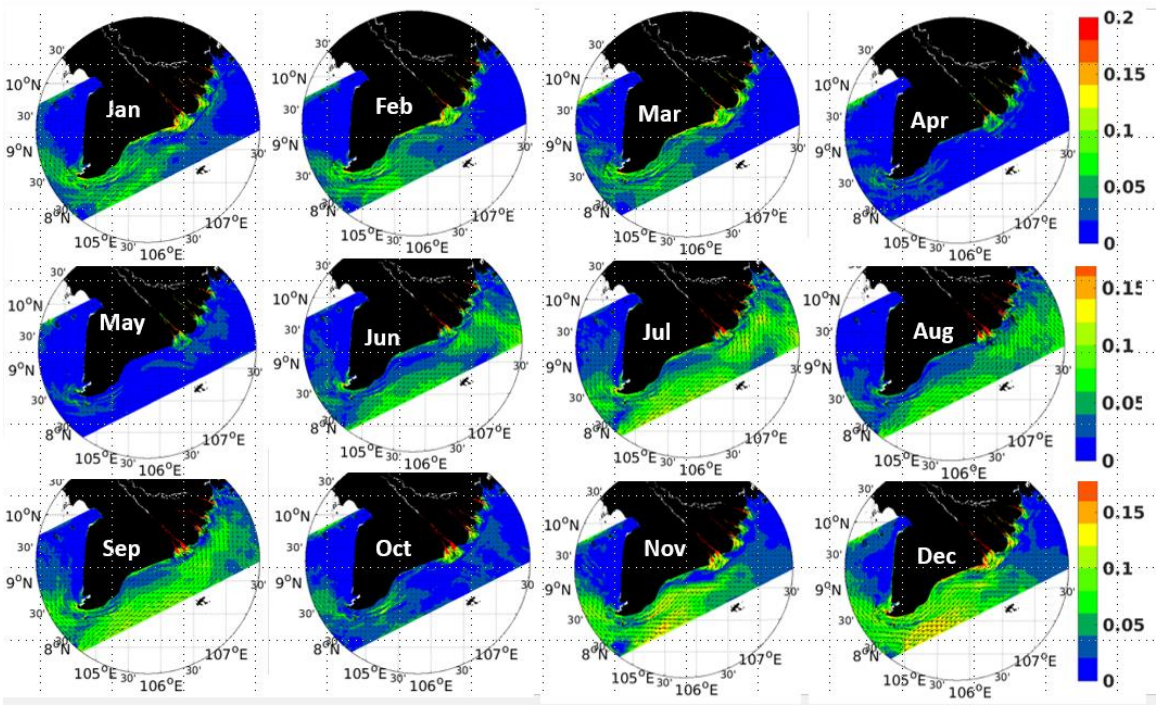

Figure 9. Monthly average bottom velocity fields (m/s) in 2014.

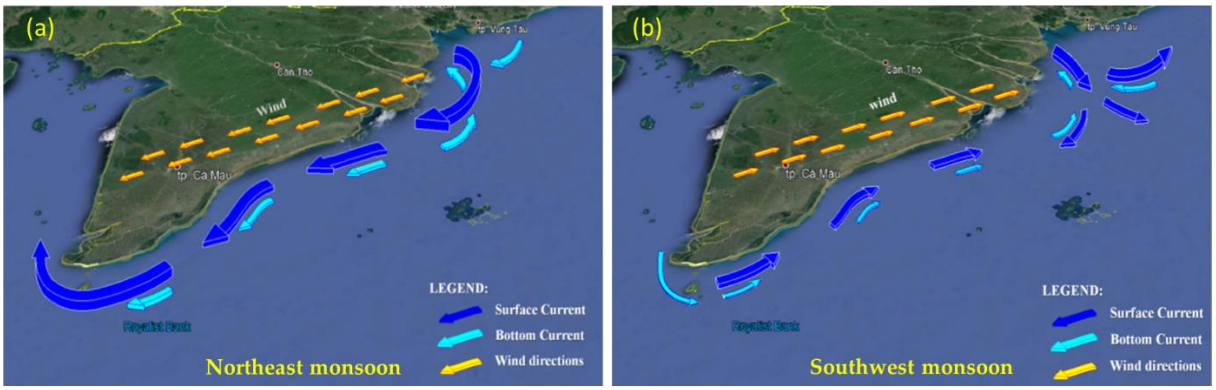

Figure 10. Proposed conceptual model of the coastal flow structure in the LMDCZ. (a) during the Northeast monsoon, wind stimulates downwelling-surface narrow jet of about 20-40 km of width and 5 m of thickness, and during the SW monsoon (b), wind simulates upwelling process.

5.3. Suspended sediment transport in the Mekong Delta

Figure 11 illustrates the monthly average suspended sediment fluxes for 10 sections (Figure 7A) of the LMDCZ in 2014, with those sections depicted in figure for the month of January. As expected, near the mouth of the Mekong Delta, the SSF increases from June to September,

348 which corresponds to the wet season when the river discharge and hence the sediment load are
349 highest. At the cross-section located northeast of the Dinh An and Tran De mouths (Figure 11),
350 the SSF can reach up to 2.25-2.40x10^6 tons/month. As time pass by, more suspended sediments
351 are transported by currents in a south-westerly direction from the mouth of the Mekong Delta
352 toward to the Ca Mau Cape. At the cross-section located southwest, just after the Dinh An
353 mouth, SSF increases from a value of 2.30x10^6 tons/month in October, to reach the highest
354 value of 6.36 x10^6 tons/month in December. During this month, SSFs are the highest of the year
355 for all coastal sections. In the East Sea, offshore from the Ca Mau Cape, SSF reaches a value
356 of 5.32x10^6 tons/month and goes into the West Sea with a value of 5.89 x10^6 tons/month. SSF
357 decrease from January to March and during the inter-season (April and May), SSF is nearly
358 insignificant. The analysis of the sediment budget was calculated for the 10 sections of the
359 LMDCZ mentioned above, with Table 2A presenting the sediment budget for each of those
360 sections as estimated by the CROCO model, with negative and positive values representing
361 zones of erosion and accretion, respectively. The zones of erosion and accretion, as determined
362 by the model are also depicted in Figure 12. It can be seen that sections S2, S4, and S9 have
363 experienced erosion according to the model (Figure 7A), which agrees with the observed
364 shoreline changes observed from 1990 to 2015 also show agreement between the model and
365 observations for section S3, S4, and S9 (Marchesiello *et al.* 2019). In section S3, erosion area
366 is calculated for the East Sea before the Ca-Mau Cape, an accretion area just behind it in the
367 West Sea, and then an erosion area in the North of the section. Thus, this makes the sediment
368 budget in this cell negative. Section S4, corresponding to the Ganh-Hao zone, is eroding during
369 most months with a sediment budget of -7.02 x 10^6 tons. Section S9, corresponding to the Go
370 Cong zone, is eroding during the Northeast winds from October to May, with a sediment budget
371 of -1.94 x 10^6 tons. According to Table 4 section S2, which extends from the Ca Mau Cape
372 experiences accretion, in agreement with observations. Section S1 in the West Sea is
373 experiencing erosion according to observations, but this is not seen in the model simulation.

374 The yearly computed sediment budget of this section is almost null, i.e., no erosion nor
375 accretion occurs. The reason for this disagreement is likely because of the impact of subsidence
376 with a rate of 20 mm/year in this area, the highest in the LMD, which is not yet taken into
377 consideration by the CROCO model.

378

379 Hein et al. (2013) modelled the dynamics of sediments in the ROFI of the Mekong Delta and,
380 as in Hordoir et al. (2006), confirmed the important role that the seasonal cycle of river
381 discharge and monsoonal winds play on the Mekong Delta; their study, however, focused on
382 sediment deposition and not on the characteristics of the freshwater plume. Previous studies
383 have shown the deposition of fine sediments over the continental shelf during the SW monsoon
384 season due to high river discharge. Their model further suggests that sediment deposition also
385 occurs during the low flow season, but it is limited to areas near the river mouth, where the
386 delta is still expanding, and that the wind driven circulation, waves, and tidal action cause net
387 erosion in other parts of the Lower Mekong Delta Coastal Zone. Even though the net transport
388 of fine sediments is to the south, i.e., towards the Gulf of Thailand, in the southern part of the
389 delta, there is a negative sediment budget due to the strong coastal current causing coastal
390 erosion and hence shoreline retreat, evidence for which is presented in Karlsrud *et al.* (2017).
391 This strong coastal current during the northeast winter monsoon, flowing in the direction of the
392 propagating Kelvin wave, was also observed in the modelling study of Hordoir *et al.* (2006).

393

394 Hein *et al.* (2013) recommended further studies to examine the influence of hydropower dams
395 in the upper catchment of the Mekong River as well as the impacts of climate change. This was
396 also stressed more recently by Li *et al.* (2017) who mentioned that our understanding of the
397 evolution of the delta over the past 50 years is not adequate to respond to the impacts of climate
398 change. Accordingly, they used Landsat data over the period 1973-2015 and found that the
399 majority of the delta is experiencing erosion, particularly to the East of the Ca Mau Peninsula

and the north-western side of the delta in the Gulf of Thailand and that overall, the Mekong Delta has experienced a shift from a growing to a shrinking region around the year 2005.

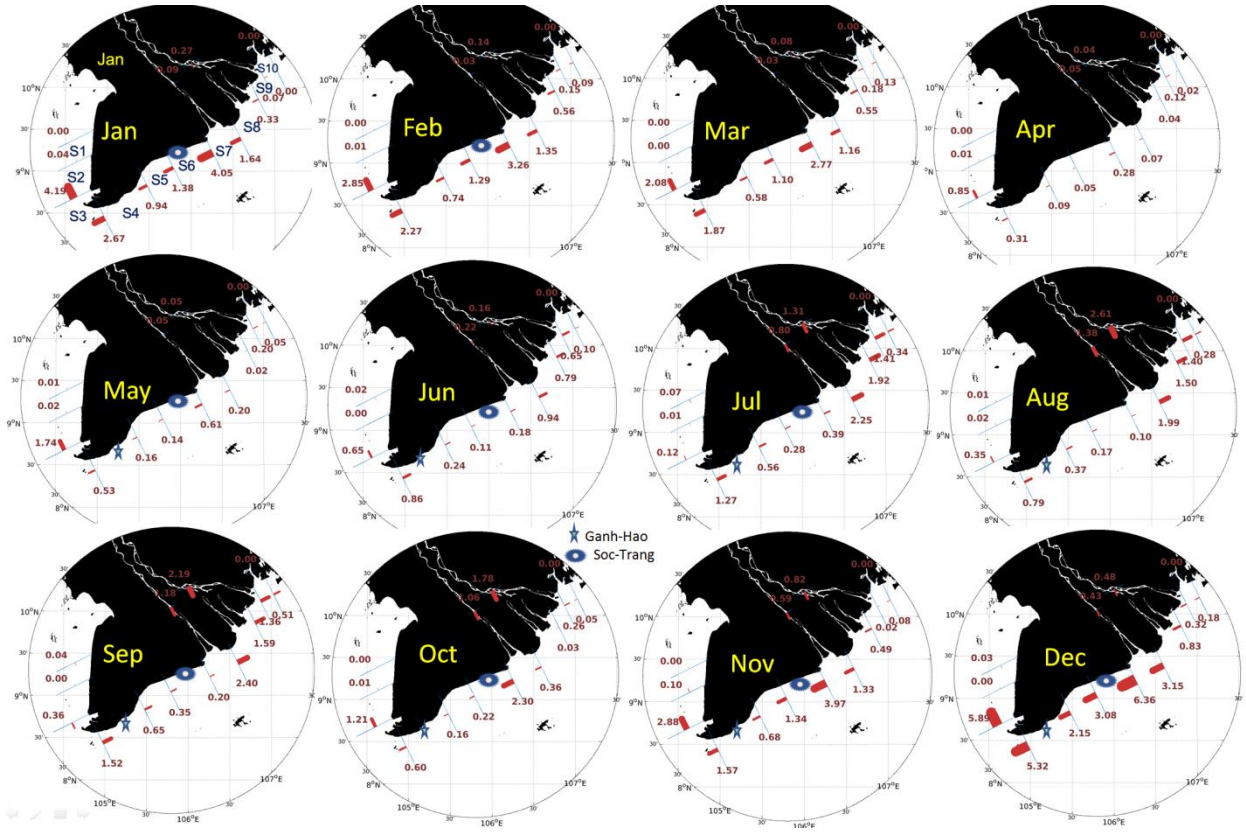

Figure 12. Monthly average suspended sediment fluxes (10^6 tons/month) at different cross-sections of the LMDCZ

6. Conclusions

In this study, the three-dimensional CROCO model was used to simulate the circulation and transport of sediments in the ROFI of the Mekong Delta. The model was validated using *in situ* measurements, including significant wave height, tidal levels, and salinity profiles. The flow structure obtained using a 30-layer vertical grid closely agrees with the conceptual model proposed in relation to conditions either favouring upwelling or downwelling under seasonally varying wind direction. During the SW monsoon when the winds are favourable to upwelling, large volumes of freshwater flow out of the various rivers flowing into the Mekong Delta. When the North-eastern winds prevail, which favour downwelling, Ekman transport pushes the current against the coast, resulting in a narrow surface coastal jet, 25-40 km wide and 5 m thick.

This coastal jet allows for the transportation of suspended sediments toward the Ca Mau Cape and further into the West Sea.

A sediment budget analysis was performed to identify zones prone to accretion and erosion in the coastal zone of the LMD and to inform the development of preventive actions against coastal erosion and the wider integrated coastal management agenda in the region. The results of this analysis showed good agreement with an erosion map obtained from the Southern Institute of Water Resources Research (SIWRR), confirming the suitability of the model for further simulation. It is recommended that the model be used in further research to simulate the impacts of different scenarios of changes in river discharge due to anthropogenic alterations of the river flow or as a result of climate change, sand mining and sea level rise on the processes and dynamics of the ROFI and sediment transport in the delta.

Authorship statement

Nguyet-Minh Nguyen, Dinh Cong San, Kim Dan Nguyen: Conceptualization, Methodology, Software, Validation, Visualisation, Formal analysis, Investigation, Original draft preparation.

Quoc Bao Pham, Alexandre S. Gagnon, Duong Tran Anh: Supervision, Conceptualization, Methodology, Final draft preparation, reviewing and Editing.

Declaration of competing interest

The authors reported no potential competing interest

Acknowledgments

The results presented in this paper were obtained as part of the LMDCZ Project financed by the *Agence Française de Développement* (AFD) and the European Union. We would like to thank the VITEL project team for sharing the CTD measurements. We also thank the Fulbright U.S.

– ASIAN visiting scholar program (G-1-00005) for awarding a research exchange to Dr Duong Tran Anh at the University of South Florida, USA, in the summer of 2021. The authors greatly appreciate the Editor and also deeply thank the anonymous reviewers for their constructive comments to improve the final version of te manuscript.

References

Anthony, E.J., Brunier, G., Besset, M., Goichot, M., Dussouillez, P., Nguyen, V.L., 2015. Linking rapid erosion of the Mekong river delta to human activities. Sci. Rep. 5, 14745.

Avicola, G. and Huq, P., 2003a. The characteristics of the recirculating bulge region in coastal buoyant outflows. *Journal of Marine Research*, *61*(4), pp.435-463.

Avicola, G. and Huq, P., 2003b. The role of outflow geometry in the formation of the recirculating bulge region in coastal buoyant outflows. *Journal of marine research*, *61*(4), pp.411-434.

Blaas, M., Dong, C., Marchesiello, P., McWilliams, J.C. and Stolzenbach, K.D., 2007. Sediment-transport modeling on Southern Californian shelves: A ROMS case study. *Continental shelf research*, *27*(6), pp.832-853.

Boretti, A., 2020. Implications on food production of the changing water cycle in the Vietnamese Mekong Delta. *Global Ecology and Conservation*, *22*, p.e00989.

Buschmann, J., Berg, M., Stengel, C., Winkel, L., Sampson, M.L., Trang, P.T.K. and Viet, P.H., 2008. Contamination of drinking water resources in the Mekong delta floodplains: Arsenic and other trace metals pose serious health risks to population. *Environment International*, *34*(6), pp.756-764.

Campbell, I.C., 2012. Biodiversity of the Mekong delta. In *The Mekong Delta System* (pp. 293-313). Springer, Dordrecht.

Chao, S.-Y. 1990. Tidal modulation of estuarine plumes. *Journal of Physical Oceanography*, 20(7), 1115–1123.

Chen, C., Lai, Z., Beardsley, R.C., Xu, Q., Lin, H. and Viet, N.T., 2012. Current separation and upwelling over the southeast shelf of Vietnam in the South China Sea. Journal of Geophysical Research: Oceans, 117(C3).

Cochrane, T.A., Arias, M.E. and Piman, T., 2014. Historical impact of water infrastructure on water levels of the Mekong River and the Tonle Sap system. *Hydrology and Earth System Sciences*, *18*(11), pp.4529-4541.

De Boer, G.J., Pietrzak, J.D. and Winterwerp, J.C., 2006. On the vertical structure of the Rhine region of freshwater influence. *Ocean dynamics*, *56*(3), pp.198-216.

de Kok, J.M. 1996. A two-layer model of the Rhine plume. *Journal of marine Systems*, 8, 269–284.

Debreu, L., Auclair, F., Benshila, R., Capet, X., Dumas, F., Julien, S. and Marchesiello, P., 2016, April. Multiresolution in CROCO (Coastal and Regional Ocean Community model). In *EGU General Assembly Conference Abstracts* (pp. EPSC2016-15272).

Debreu, L., Marchesiello, P., Penven, P. and Cambon, G., 2012. Two-way nesting in split-explicit ocean models: Algorithms, implementation and validation. *Ocean Modelling*, *49*, pp.1-21.

Dong, J., Fox‐Kemper, B., Zhu, J. and Dong, C., 2021. Application of symmetric instability parameterization in the Coastal and Regional Ocean Community Model (CROCO). *Journal of Advances in Modeling Earth Systems*, *13*(3), p.e2020MS002302.

Fong, D.A. and Geyer, W.R., 2001. Response of a river plume during an upwelling favorable wind event. *Journal of Geophysical Research: Oceans*, *106*(C1), pp.1067-1084.

Fong, D.A. and Geyer, W.R., 2002. The alongshore transport of freshwater in a surface-trapped river plume. *Journal of Physical Oceanography*, *32*(3), pp.957-972.

Garcia Berd´eal, I., Hickey, B.M., & Kawase, M. 2002. Influence of wind stress and ambient

Geyer, W., and G. Kineke. 1995. Observations of currents and water properties in the Amazon frontal zone, *J. Geophys. Res.*, 100, 2321–2339.

Geyer, W.R., Signell, R.P., Fong, D.A., Wang, J., Anderson, D.M. and Keafer, B.A., 2004. The freshwater transport and dynamics of the western Maine coastal current. *Continental Shelf Research*, *24*(12), pp.1339-1357.

Guong, V.T. and Hoa, N.M., 2012. Aquaculture and agricultural production in the Mekong Delta and its effects on nutrient pollution of soil and water. In *The Mekong Delta System* (pp. 363-393). Springer, Dordrecht.

493 Hein, B., 2013. Processes of stratification and destratification in the Mekong ROFI-seasonal and
494 intraseasonal variability (Doctoral dissertation, Staats-und Universitätsbibliothek Hamburg Carl von
495 Ossietzky).
496 Hein, H., Hein, B. and Pohlmann, T., 2013. Recent sediment dynamics in the region of Mekong water
497 influence. *Global and Planetary Change*, *110*, pp.183-194.
498 Hickey, B.M., Pietrafesa, L.J., Jay, D.A. and Boicourt, W.C., 1998. The Columbia River plume study:
499 Subtidal variability in the velocity and salinity fields. *Journal of Geophysical Research: Oceans*, *103*(C5), pp.10339-10368.
501 Hordoir, R., Nguyen, K.D. and Polcher, J., 2006. Simulating tropical river plumes, a set of
502 parametrizations based on macroscale data: A test case in the Mekong Delta region. *Journal of*
503 *Geophysical Research: Oceans*, *111*(C9).
504 Horner-Devine, A.R., Hetland, R.D. and MacDonald, D.G., 2015. Mixing and transport in coastal river
505 plumes. *Annual Review of Fluid Mechanics*, *47*, pp.569-594.
506 Horner-Devine, A.R., Jay, D.A., Orton, P.M. and Spahn, E.Y., 2009. A conceptual model of the strongly
507 tidal Columbia River plume. Journal of Marine Systems, 78(3), pp.460-475.
508 IRD, "Franco-Vietnamese Oceanographic Campaigns with the ALIS Research Vessel of the French
509 Institute of Research for Development - June 19 to July 12, 2014," *Final Report,* 2014.
510 Joseph, A., 2017. Investigating Seafloors and Oceans: From Mud Volcanoes to Giant Squid. Elsevier.
511 https://doi.org/10.1016/C2015-0-05842-7
512 Karlsrud, K., Vangelsten, B.V. and Frauenfelder, R., 2017. Subsidence and shoreline retreat in the Ca
513 Mau Province–Vietnam. Causes, consequences and mitigation options. *Geotechnical Journal of the*
514 *SEAGS & AGSSEA*, *48*.
515 Kondolf, G.M., Rubin, Z.K. and Minear, J.T., 2014. Dams on the Mekong: Cumulative sediment
516 starvation. *Water Resources Research*, *50*(6), pp.5158-5169.
517 Large, W.G., McWilliams, J.C. and Doney, S.C., 1994. Oceanic vertical mixing: A review and a model
518 with a nonlocal boundary layer parameterization. *Reviews of geophysics*, *32*(4), pp.363-403.

519 Le Xuan, T., Thanh, V.Q., Reyns, J., Van, S.P., Anh, D.T., Dang, T.D. and Roelvink, D., 2019.
520 Sediment transport and morphodynamical modeling on the estuaries and coastal zone of the Vietnamese
521 Mekong Delta. Continental Shelf Research, 186, pp.64-76.
522 Li, X., Liu, J.P., Saito, Y. and Nguyen, V.L., 2017. Recent evolution of the Mekong Delta and the
523 impacts of dams. *Earth-Science Reviews, 175*, pp.1-17.
524 Marchesiello, P., McWilliams, J.C. and Shchepetkin, A., 2001. Open boundary conditions for long-
525 term integration of regional oceanic models. *Ocean Modelling*, *3*(1-2), pp.1-20.
526 Marchesiello, P., Nguyen, N.M., Gratiot, N., Loisel, H., Anthony, E.J., San Dinh, C., Nguyen, T.,
527 Almar, R. and Kestenare, E., 2019. Erosion of the coastal Mekong delta: Assessing natural against man
528 induced processes. *Continental Shelf Research*, *181*, pp.72-89.
529 Meade, R.H., 1996. River-Sediment Inputs to Major Deltas. In: J.D. Milliman and B.U. Haq (Editors),
530 Sea-Level Rise and Coastal Subsidence: Causes, Consequences, and Strategies. Springer Netherlands,
531 Dordrecht, pp. 63-85.
532 Minderhoud, P.S.J., Erkens, G., Pham, V.H., Bui, V.T., Erban, L., Kooi, H., Stouthamer, E., 2017.
533 Impacts of 25 years of groundwater extraction on subsidence in the Mekong delta, Vietnam.
534 Environmental Research Letters 12(6), 064006.
535 Nhan, N.H. and Cao, N.B., 2019. Damming the Mekong: Impacts in Vietnam and solutions. In *Coasts*
536 *and Estuaries* (pp. 321-340). Elsevier.
537 Pardo, P.C., Padín, X.A., Gilcoto, M., Farina-Busto, L. and Pérez, F.F., 2011. Evolution of upwelling
538 systems coupled to the long-term variability in sea surface temperature and Ekman transport. Climate
539 Research, 48(2-3), pp.231-246.
540 Pimenta, F.M. and Kirwan Jr, A.D., 2014. The response of large outflows to wind forcing. *Continental*
541 *Shelf Research*, *89*, pp.24-37.
542 Pimenta, F.M., Kirwan Jr, A.D. and Huq, P., 2011. On the transport of buoyant coastal plumes. *Journal*
543 *of Physical Oceanography*, *41*(3), pp.620-640.
544 Price, J.F., Weller, R.A. and Schudlich, R.R., 1987. Wind-driven ocean currents and Ekman
545 transport. Science, 238(4833), pp.1534-1538.

546 Rubin, Z.K., Kondolf, G.M., Carling, P.A., 2015. Anticipated geomorphic impacts from Mekong basin
547 dam construction. International Journal of River Basin Management 13(1), 105-121.
548 Sarmiento, J.L. and Gruber, N., 2006. *Ocean biogeochemical dynamics*. Princeton University Press.
549 ISBN 978-0-691-01707-5
550 Schmidt, C., 2015. Alarm over a sinking delta. Science 348(6237), 845-846
551 Shchepetkin, A.F. and McWilliams, J.C., 2003. A method for computing horizontal pressure‐gradient
552 force in an oceanic model with a nonaligned vertical coordinate. *Journal of Geophysical Research:*
553 *Oceans*, *108*(C3).
554 Shchepetkin, A.F. and McWilliams, J.C., 2005. The regional oceanic modeling system (ROMS): a split-
555 explicit, free-surface, topography-following-coordinate oceanic model. *Ocean modelling*, *9*(4), pp.347-
556 404.
557 Simpson, J. H. and A. Snidvongs, 1998. The influence of monsoonal river discharge on tropical shelf
558 seas: the Gulf of Thailand as a case for study. Proceedings of the International Workshop on the Mekong
559 Delta at Chiang Rai on 23–27 February 1998, 86–99.
560 Simpson, J.H., 1997. Physical processes in the ROFI regime. Journal of marine systems, 12(1-4), pp.3-
561 15.
562 Simpson, J.H., Williams, E., Brasseur, L.H. and Brubaker, J.M., 2005. The impact of tidal straining on
563 the cycle of turbulence in a partially stratified estuary. *Continental Shelf* Research, 25(1), pp.51-64.
564 Smajgl, A., Toan, T.Q., Nhan, D.K., Ward, J., Trung, N.H., Tri, L.Q., Tri, V.P.D., Vu, P.T., 2015.
565 Responding to rising sea levels in the Mekong Delta. Nature Climate Change 5(2), 167-174
566 Soufflet, Y., Marchesiello, P., Lemarié, F., Jouanno, J., Capet, X., Debreu, L. and Benshila, R., 2016.
567 On effective resolution in ocean models. *Ocean Modelling*, *98*, pp.36-50.
568 Southern Institute of Water Resources Research (SIWRR). 2018. Erosion processes in the Lower
569 Mekong Delta Coastal Zones and measures for protecting Go-Cong and Phu-Tan, Final Report, AFD,
570 Vietnam.
571 Thanh, V.Q., Reyns, J., Wackerman, C., Eidam, E.F. and Roelvink, D., 2017. Modelling suspended
572 sediment dynamics on the subaqueous delta of the Mekong River. *Continental Shelf Research*, *147*,
573 pp.213-230.

574 Thomas, P.J. and Linden, P.F., 2010. Laboratory modelling of the effects of temporal changes of
575 estuarine-fresh-water discharge rates on the propagation speed of oceanographic coastal
576 currents. *Journal of fluid mechanics*, *664*, p.337.
577 Wang, D., Wang, H., Li, M., Liu, G. and Wu, X., 2013. Role of Ekman transport versus Ekman pumping
578 in driving summer upwelling in the South China Sea. Journal of Ocean University of China, 12(3),
579 pp.355-365.
580 Warner, J.C., Sherwood, C.R., Signell, R.P., Harris, C.K. and Arango, H.G., 2008. Development of a
581 three-dimensional, regional, coupled wave, current, and sediment-transport model. *Computers &*
582 *geosciences*, *34*(10), pp.1284-1306.
583 Whitney, M.M. and Garvine, R.W., 2005. Wind influence on a coastal buoyant outflow. *Journal of*
584 *Geophysical Research: Oceans*, *110*(C3).
585 Wolanski, E., Huan, N.N., Nhan, N.H. and Thuy, N.N., 1996. Fine-sediment dynamics in the Mekong
586 River estuary, Vietnam. Estuarine, Coastal and Shelf Science, 43(5), pp.565-582.
587 Xing, J. and Chen, S., 2017. A process study of the interaction of tidal currents, tidal mixing and density
588 gradients in a region of freshwater influence. *Journal of Marine Systems*, *172*, pp.51-63.
589 Yankovsky, A.E., Hickey, B.M. and Münchow, A.K., 2001. Impact of variable inflow on the dynamics
590 of a coastal buoyant plume. *Journal of Geophysical Research: Oceans*, *106*(C9), pp.19809-19824.
591 Yao, H.Y., Leonardi, N., Li, J.F. and Fagherazzi, S., 2016. Sediment transport in a surface-advected
592 estuarine plume. *Continental Shelf Research*, *116*, pp.122-135.
593 Yuan, Y., Horner-Devine, A.R., Avener, M. and Bevan, S., 2018. The role of periodically varying
594 discharge on river plume structure and transport. *Continental Shelf Research*, *158*, pp.15-25.
595 Ziv, G., Baran, E., Nam, S., Rodríguez-Iturbe, I. and Levin, S.A., 2012. Trading-off fish biodiversity,
596 food security, and hydropower in the Mekong River Basin. *Proceedings of the National Academy of*
597 *Sciences*, *109*(15), pp.5609-5614.
598 Johnson, G.C., Schmidtko, S. and Lyman, J.M., 2012. Relative contributions of temperature and salinity
599 to seasonal mixed layer density changes and horizontal density gradients. *Journal of Geophysical*
600 *Research: Oceans*, *117*(C4).
601 Chaufray, J.Y., Gonzalez-Galindo, F., Forget, F., Lopez-Valverde, M., Leblanc, F., Modolo, R., Hess,
602 S., Yagi, M., Blelly, P.L. and Witasse, O., 2014. Three-dimensional Martian ionosphere model: II. Effect

603 of transport processes due to pressure gradients. *Journal of Geophysical Research: Planets*, *119*(7),
604 pp.1614-1636.
605
606
607

Supplementary data (Appendix).

Table 1A. Seasonal variations in prevailing winds over the Mekong Delta and associated climatic conditions.

Cool and dry		**Hot and dry**		**Wet**						**Cool and dry**		
Jan	**Feb**	**Mar**	**Apr**	**May**	**Jun**	**Jul**	**Aug**	**Sep**	**Oct**	**Nov**	**Dec**	
NE Monsoon		**Transition**		**SW Monsoon**					**Transition**	**NE Monsoon**		

Table 2A. Monthly sediment budget (10^6 tons) in the different sections of the LMDCZ (see Figure – January - for their position) estimated by the CROCO model in 2014.

	Jan	Feb	Mar	Apr	May	Jun	Jul	Aug	Sep	Oct	Nov	Dec	Sum
S1	0.04	0.01	-0.01	0.01	0.02	0.03	0.06	0.01	0.06	0.01	0.10	0.04	0.37
S2	4.16	2.85	2.09	0.84	1.72	0.65	0.15	0.33	-0.38	1.21	2.78	5.89	22.28
S3	-1.53	-0.58	-0.21	-0.54	-1.22	-1.51	-1.41	-1.15	-1.16	-0.61	-1.31	-0.56	-11.79
S4	-1.72	-1.53	-1.29	-0.22	-0.37	0.61	0.72	0.42	0.87	-0.44	-0.89	-3.18	-7.02
S5	0.43	0.54	0.52	-0.04	-0.02	0.14	0.28	0.19	0.30	0.07	0.66	0.94	4.02
S6	2.68	1.97	1.67	0.23	0.47	-0.08	-0.11	0.08	0.15	2.08	2.63	3.28	15.03
S7	2.51	1.94	1.64	0.27	0.46	0.98	2.66	3.28	3.39	3.00	3.24	3.65	27.02
S8	1.58	0.94	0.70	0.07	0.23	0.31	1.64	3.11	3.02	2.12	1.66	2.80	18.19
S9	-0.41	-0.41	-0.36	-0.17	-0.23	0.14	0.52	0.10	0.23	-0.30	-0.52	-0.51	-1.94
S10	0.07	-0.05	-0.06	0.15	0.26	0.55	1.07	1.12	0.85	0.32	0.11	-0.14	4.25

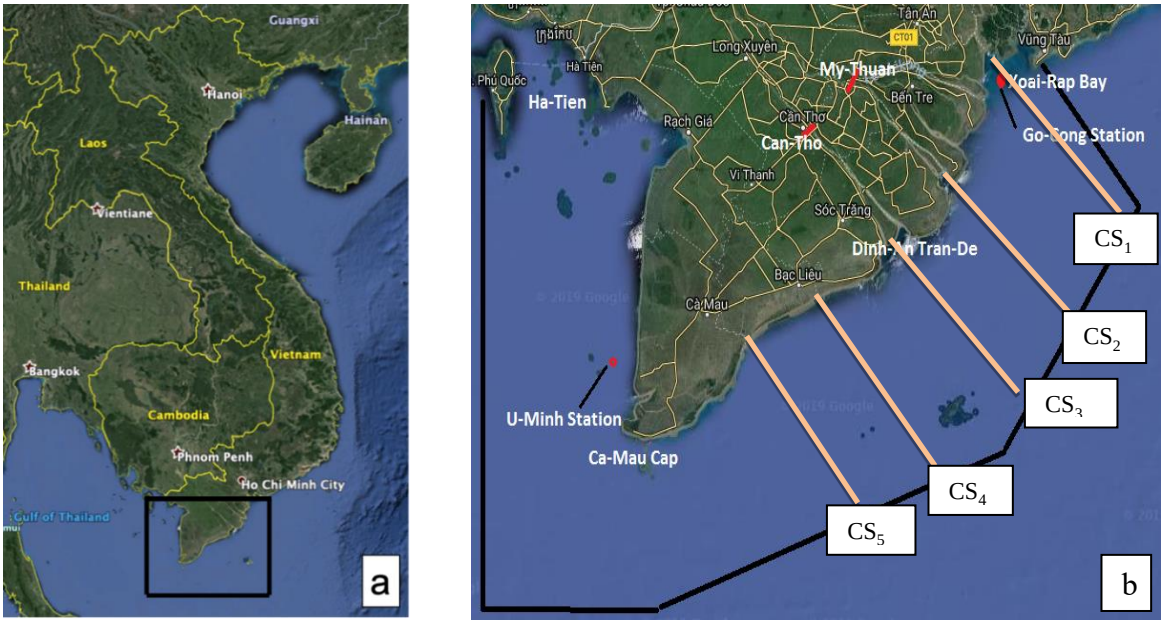

Figure 1A. a) Location of the LMDCZ and b) computational domain of the CROCO model over the Mekong Delta, showing the two upstream open boundaries at Can Tho and My Thuan, and the sea open boundaries at Go Cong and U Minh. $CS_{1\text{-}5}$ refer to the location of the fiver cross-sections referred to in the text.

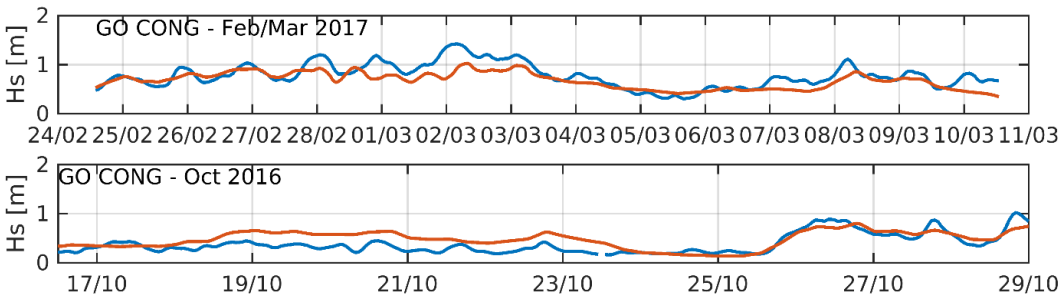

Figure 2A. Significant wave height (Hs) as simulated by the model and observed at Go Cong during the 15-day field campaign extending from February 24 to March 11, 2017 (top panel), and the 15-day field campaign on October 16-31, 2016 (bottom panel).

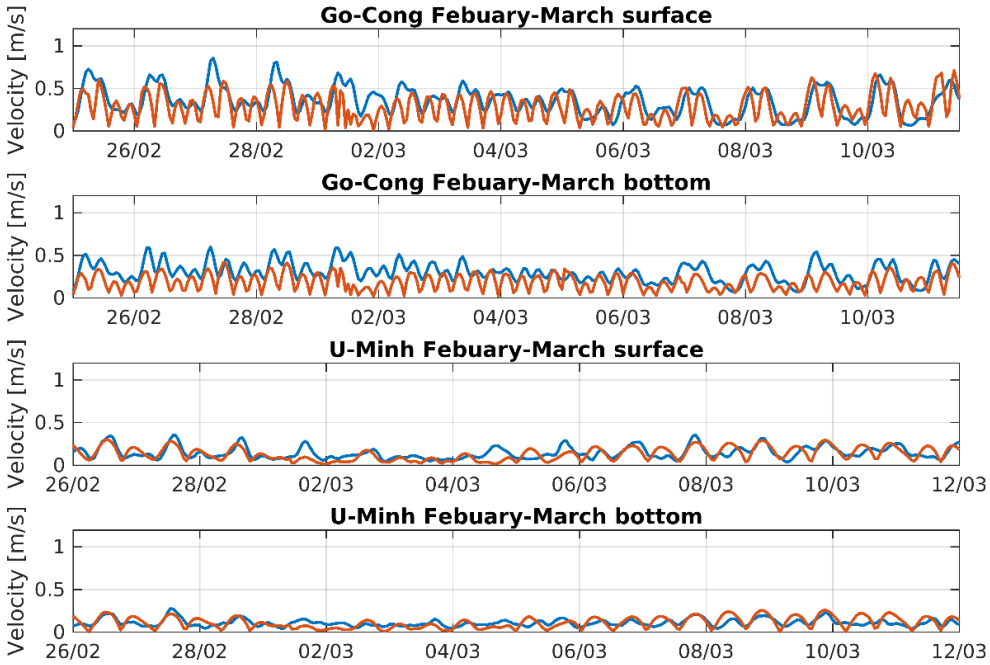

625

626 **Figure 3A.** Modelled and observed current velocity during the 15-day field campaign from
627 February 24 to March 11, 2017, at the surface and the bottom of the sea at U Minh and Go
628 Cong.

629

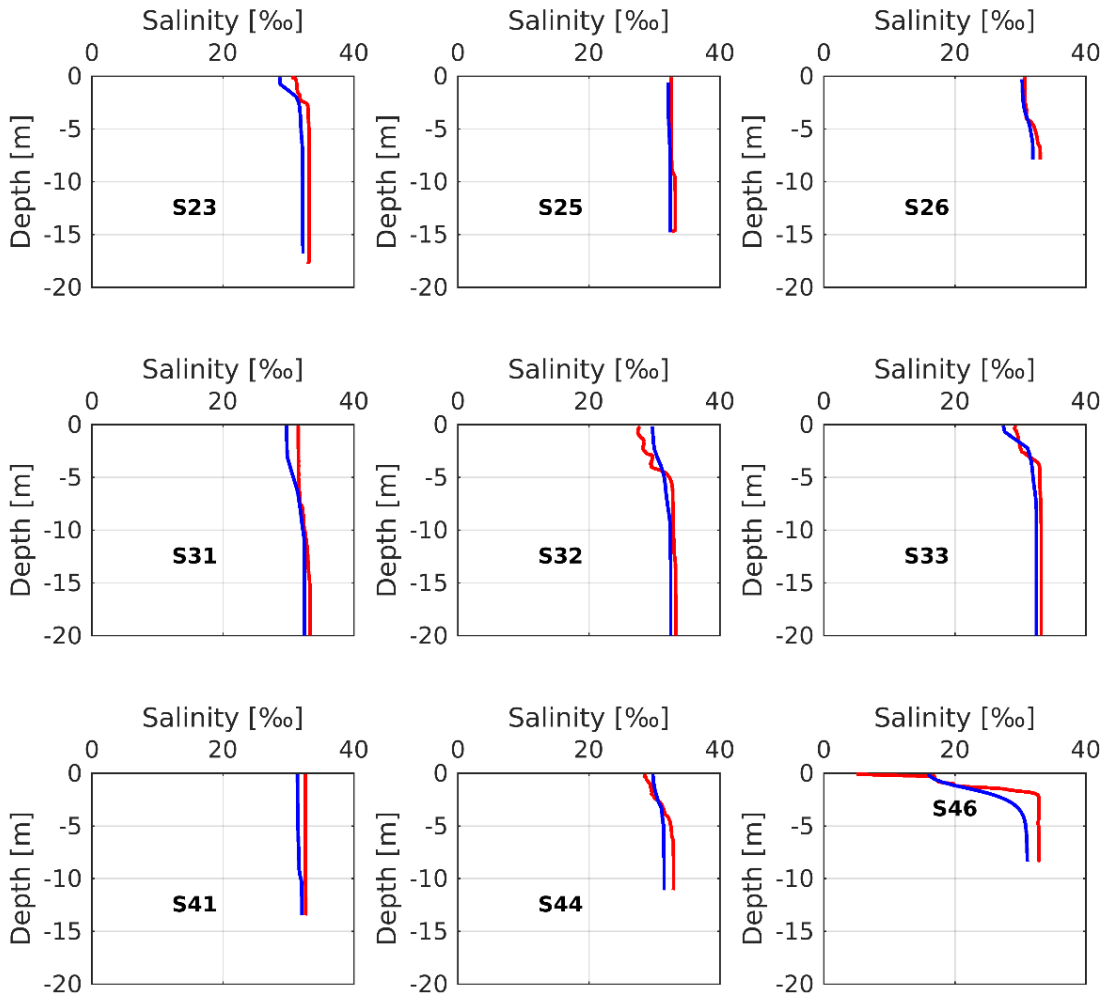

630

631 **Figure 4A**. Comparison of the salinity profile simulated (blue curves) and observed (red curves)

632 during the field measurements taken as part of the VITEL project in June 2014 at different

633 locations.

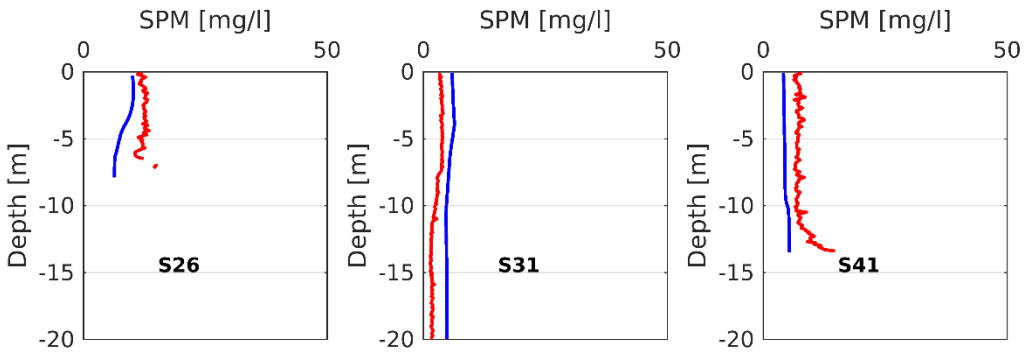

634

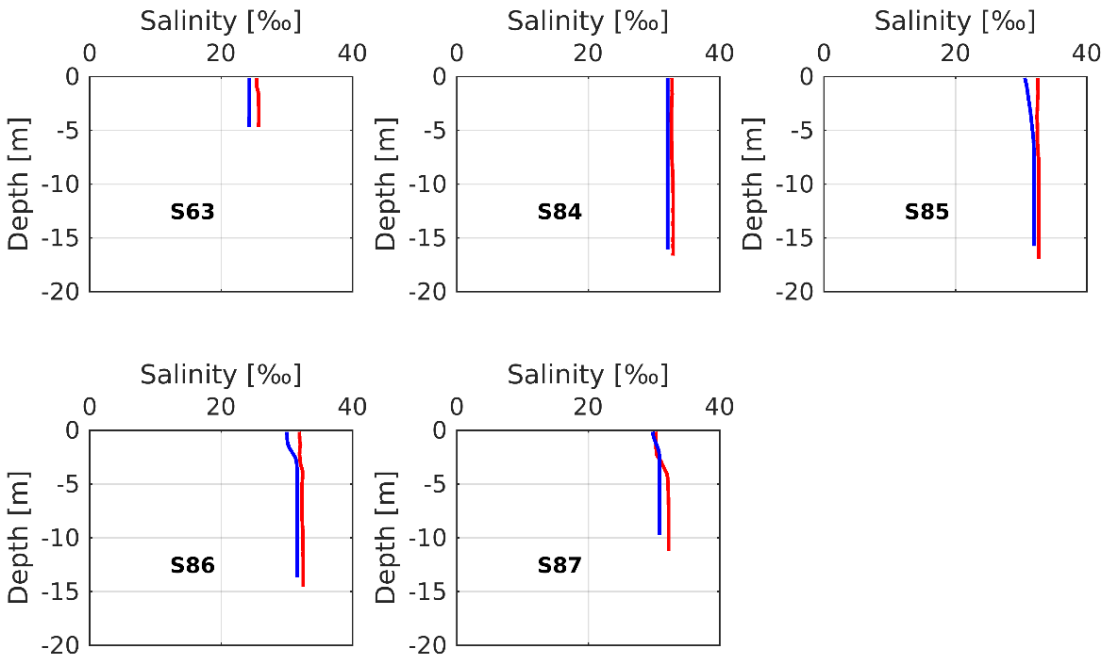

Figure 5A. Comparison of the salinity profile simulated (blue curves) and observed (red curves) during the field measurements taken as part of the LMDCZ project in February-March 2017 at different locations.

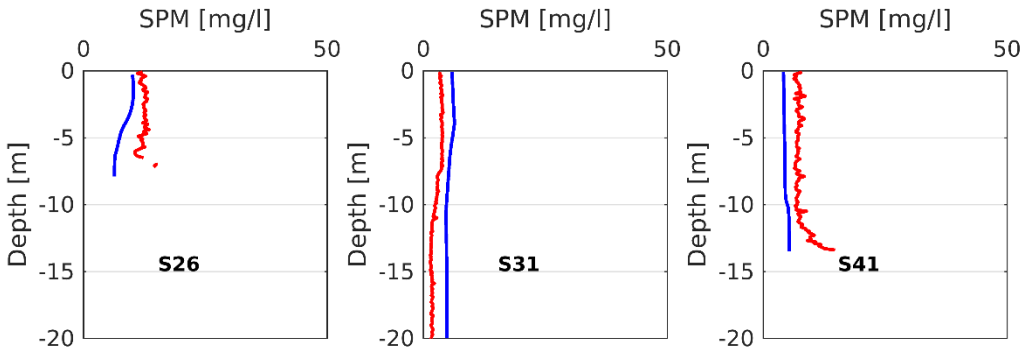

Figure 6A. Comparison of the instantaneous SPM profile simulated by the CROCO model (blue curves) and observed in June 2014 by the VITEL project field measurements (red curves).

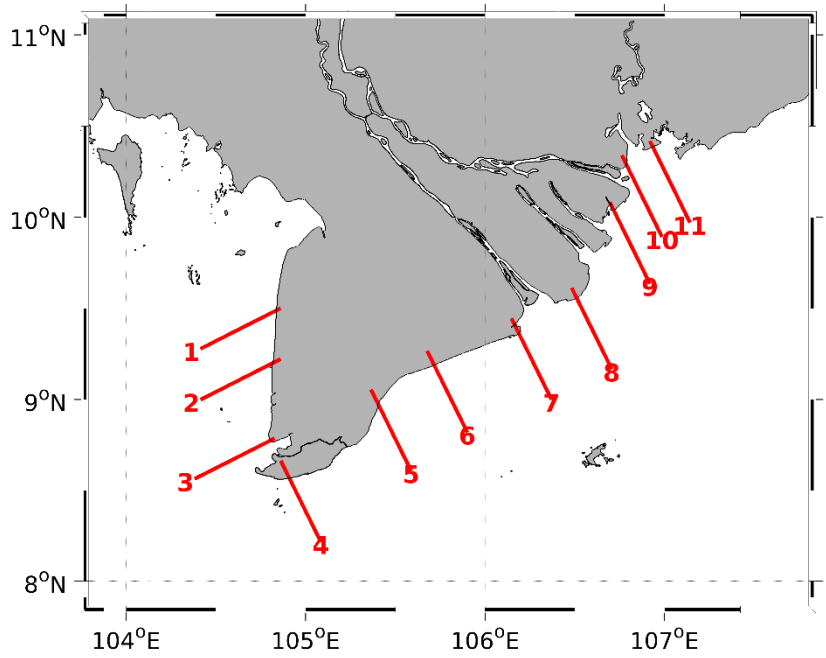

Figure 7A. The location of ten sections (S1 – S10) for extracting suspended sediment fluxes